State-specific mobility of excited cadmium and calcium ions in a discharge plasma measured by a tunable diode laser

Hirokazu Hori, Yoshihiro Ono,* Akio Watanabe,† Makoto Nakamura,‡ Yukio Inoue, and Takeki Sakurai
Department of Electric Engineering and Computer Science, Yamanashi University, Kofu 400, Japan
(Received 6 January 1992; revised manuscript received 17 August 1992)

The state-specific drift velocity of Ca^+ ions in the $3\,^2D_{3/2}$ metastable state and of Cd^+ in the $6\,^2P_{3/2}$ highly excited state in a helium glow-discharge plasma have been precisely measured by using a tunable single-mode diode laser and the state-specific mobility of excited ions has been discussed. The results show that the mobility of Ca^+ ions in the metastable state is determined by momentum-loss collisions and is almost identical with the value for Ca^+ in the ground state. In the experiment with a thin cylindrical tube, the apparent value of the mobility is dependent on the diffusion in the radial direction. On the other hand, the apparent mobility of Cd^+ ions in the $6\,^2P_{3/2}$ state is much smaller than the calculated result for Cd^+ in the ground state, but the value increases significantly with Cd vapor density. This is explained by the fact that Cd^+ ions in the $6\,^2P_{3/2}$ highly excited state decay quickly by the radiative process and the apparent mobility of the Cd^+ ions in this state in the plasma is dependent not only on the radiative lifetime but also on the excitation mechanisms for the state.

PACS number(s): 52.25.−b, 35.80.+s, 51.50.+v

I. INTRODUCTION

The drift velocity is an important measure of transport properties of ions in plasma and is usually estimated from mobility data provided by the drift-tube method. In the drift-tube experiments, ions transport in an atmosphere approximating an ideal of neutral and uniform gas with uniform electric field applied, so that results obtained are compared directly with theory and provide precise values of ion mobility and collision cross section [1,2]. The ionic drift velocity in plasma is defined, in the same way as in neutral gas, as the average velocity of ions along electric field applied through the plasma, however, the transport properties of ions in plasma are complicated substantially.

Ion collisions in plasma are not only with ground-state neutral atoms but also with metastable neutral atoms and various kinds of charged particles involved in continuous ionization, recombination, and excitation processes keeping the stationary plasma. Among these, the elastic collisions resulting in no change in the ionic internal state can be accounted for by including corresponding collision terms in the equation of macroscopic motion of the ion species in the usual way as neutral atoms. However, several types of collisions, such as charge-transfer and excitation-transfer collisions, which change the internal state of ions, play a very different role from simple momentum-loss collisions. First, the cross sections for these types of collisions are state dependent. Second, these collisions together with internal transition or decay of ions contribute to the kinetic property of the ion ensemble in some complicated way. A single species of ion has a number of excited states, which disappear in the drift-tube experiments in the way of transport in neutral atmosphere, and a state-specific treatment should be required in the consideration of the kinetic properties of ions in plasma. Especially, the transport of ions in a short-lived highly excited state should be dependent significantly on ionization and decay process rather than momentum-loss collisions. Although ions in highly excited states contribute a negligible amount to the average velocity of the ion species in the case of weakly ionized plasma, their transport properties have special importance when light-emission characteristics, laser action, and chemical processes in the plasma are investigated.

As well as these microscopic processes, the geometrical shape of the plasma possibly affects the ion transport in the case of the plasma confined in a relatively small envelope such as a thin discharge tube. In this case the ion transport longitudinal to the applied electric field should be perturbed by transverse diffusion and drift of ions followed by deposition and recombination at the container wall, which produce anisotropy or nonuniformity in the plasma.

When the transport properties are considered for an ion ensemble in a certain quantum state, all of the transient processes discussed above will contribute as if the collisional loss of center-of-mass momentum is increased. When the characteristic time of the population and decay processes for the considered ion ensemble is shorter than the duration of the drift motion of the ion ensemble due to true momentum-loss collisions, the drift velocity and apparent mobility should be smaller than the steady-state values expected from the mobility data or collision cross section. In this paper, the term "apparent mobility" is used for the drift velocity divided by the magnitude of the applied electric field, when the ion transport is dependent significantly on the transient phenomena discussed above.

In these respects, it is not simple to estimate the transport properties of ions in plasma from mobility data based on the drift-tube method. In fact, several authors have reported the drift-velocity and mobility measurements in He-Cd glow discharge for the purpose of studying lasers and have shown results in significant disagree-

ment with mobility data given by the drift-tube method [3,4]. Although most of these measurements are indirect, the results indicate the importance of the drift-velocity measurement in a live plasma. After these reports, however, little experimental data have been obtained for live discharge plasma because of technical difficulty.

Recently we have developed a technique for direct and precise measurements of state-specific drift velocity of ions in live discharge plasma, which is based on Doppler-shift measurements of an ionic absorption line by using counterpropagating laser beams from a frequency-controlled diode laser. Two absorption spectra, one redshifted and the other blueshifted due to ionic drift motion, are obtained for a pair of counterpropagating laser beams by a single sweep of the laser frequency through the ionic resonance line. The frequency difference between these spectra is exactly twice the Doppler shift due to drift motion in the direction of the laser propagation. Basically in this laser-Doppler measurement, the velocity distribution of ions in the direction of the laser propagation is obtained via Doppler profile of the ionic absorption line, so that it is not essential to assume a shifted Maxwellian distribution of ion velocity. Population density and ion temperature are obtained simultaneously from the magnitude and width of the absorption spectra. A perturbation due to laser irradiation on the plasma is very small, as is known from the optogalvanic effect. A similar optical method has been employed by Haese, Pan, and Oka for the drift-velocity measurement of a molecular ion [5].

The laser-Doppler measurement of the drift velocity has several special features. Only one species of ion in one of the quantum states, either ground or excited, is measured selectively in a complex mixture of different kinds of ions by virtue of the monochromatic laser. State-selective measurements of the drift velocity provide information not only about kinetic properties but also about effects of ionization, excitation, and relaxation processes upon ion transport. The sensitivity of absorption measurement is high by virtue of stable continuous-wave operation of the diode laser, so that the technique can be applied for ions in a highly excited state. A spatially resolved measurement is possible for a plasma with dimensions larger than the diameter of the laser beam, and spatial distributions of drift velocity, ion density, and ion temperature provide information about anisotropy of the plasma.

In this paper, we report details of the laser-Doppler measurement of drift velocity. We investigate first the state-specific drift velocity and mobility derived from the laser-Doppler measurement and clarify their relation to the ionization, excitation, and decay mechanisms according to the nature of the ionic state considered and to the plasma parameters. We report drift-velocity measurements of Ca^+ and Cd^+ ions in their excited states in a positive column of He glow discharge using $Al_xGa_{1-x}As$ lasers. In the case of the Ca^+ ion, a metastable $3\,^2D_{3/2}$ state is measured, and resulting values of state-specific mobility are in good agreement with the steady-state mobility reported in several articles. Radial distributions of drift velocity, ion density, and ion temperature are measured for He-Ca discharge tubes of several different diameters, and the effect of radial diffusion upon ion transport is studied. The result shows the apparent mobility deviates from the steady-state value with the decrease of the tube diameter. In the case of the Cd^+ ion, a highly excited $6\,^2P_{3/2}$ state is measured, and the apparent state-specific mobility changes significantly according to a change in discharge condition being affected strongly by ionization and excitation mechanisms.

II. LASER MEASUREMENT OF DRIFT VELOCITY

A. Principle of measurement

An absorption line of ions in their thermal motion is broadened inhomogeneously due to the Doppler effect and shows a Gaussian profile when its homogeneous width $\Delta\nu_h$ is small, i.e., $(\Delta\nu_h/\nu_0)^2 \ll k_B T_i/m_I c^2$, where ν_0, T_i, and m_I are ionic resonance frequency, temperature, and mass, and k_B and c the Boltzmann constant and the light velocity, respectively. In the case of the ions drifting collectively with a mean velocity v_d along an external electric field applied as shown in Fig. 1(a), the central frequency of the ionic absorption line is shifted from the ionic resonance frequency by $\nu_0(v_d/c)\cos\theta$, where θ is an angle between directions of the ionic drift motion and the light propagation. When the ionic absorption line is measured simultaneously with laser beams propagating in the same and opposite directions to the ionic drift motion, i.e., $\theta=0$ and π, one redshifted and one blueshifted spectra are observed, and the frequency difference $\Delta\nu$ between centers of these absorption spectra gives the drift velocity, as shown in Fig. 1(b), by

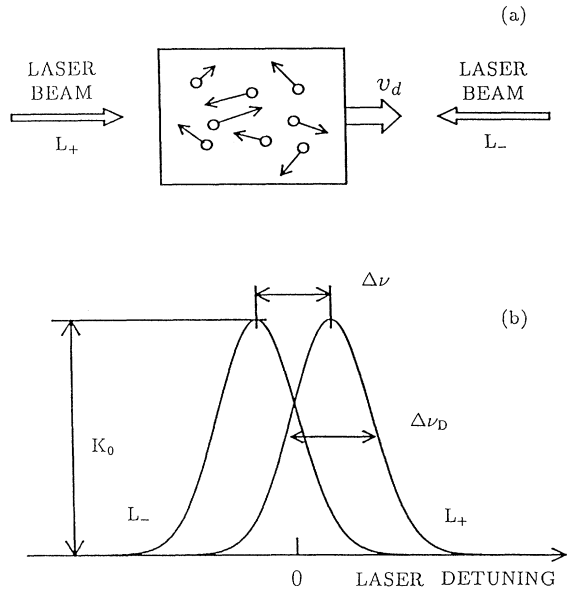

FIG. 1. (a) Ions in thermal motion drift in the $+z$ direction; and (b) absorption spectra measured by laser beams propagating in opposite directions.

$$v_d = \frac{\Delta\nu}{2\nu_0} c \ . \tag{1}$$

In addition to the drift velocity, the population density n_i and the ion temperature T_i can be measured from the peak value K_0 and the spectral width $\Delta\nu_D$ of the absorption spectra, respectively [6].

B. Interpretation of experimental data

According to state-selective nature and spatial resolution, the laser measurement of the drift velocity provides useful information not only about the transport property but also indirectly about mechanisms of ionization, excitation, and relaxation. We will discuss in the following how these mechanisms are concerned with the drift-velocity measurement.

1. Drift velocity and mobility in general definition

The drift velocity is defined as the average velocity of ions, or the velocity of the center of mass of the ion cloud, along a uniform electric field applied throughout the gas or plasma in which ions transport. In general, the drift velocity is determined as a balance of the acceleration by the electric field E and the loss of the center-of-mass velocity $v_{\text{c.m.}}$ due to collisions, and the equation of center-of-mass motion of the ion cloud is given by

$$m_I \frac{dv_{\text{c.m.}}}{dt} = qE - \Gamma_c m_I v_{\text{c.m.}} \ , \tag{2}$$

where q is the electric charge of the ion and Γ_c corresponds to the rate that the center-of-mass velocity or momentum is lost by collisions per unit time and its reciprocal gives the mean free time τ_c. After an acceleration time t_a the ion cloud initially at rest gets the center-of-mass velocity $v_{\text{c.m.}}$,

$$v_{\text{c.m.}} = \frac{qE}{m_I \Gamma_c}[1 - e^{-\Gamma_c t_a}] \ , \tag{3}$$

along the applied electric field. The steady-state value of $v_{\text{c.m.}}$ gives usual drift velocity v_d,

$$v_d = \frac{qE}{m_I \Gamma_c} \ , \tag{4}$$

and mobility μ,

$$\mu = \frac{v_d}{E} = \frac{q}{m_I \Gamma_c} \ , \tag{5}$$

which is the factor of proportionality between the steady-state drift velocity v_d and applied electric field E.

The collision rate Γ_c describes purely kinetic phenomena. In the case of ion transport in a neutral and uniform gas, Γ_c is determined by ion collisions with gaseous atoms and dependent on the averaged thermal velocity. Following the calculation given originally by Langevin cited in Ref. [7] and denoting the collision rate in this case as Γ_{cn}, one can obtain

$$\Gamma_c = \Gamma_{cn} = \frac{4}{3} \frac{m_G}{m_I + m_G} \langle \sigma_c \rangle \langle v_r \rangle n_G \ , \tag{6}$$

where m_G is the mass of gaseous atoms, σ_c is the collision cross section with neutral atoms, v_r is the relative velocity between atoms and the ion, n_G is the atomic population density, and the angular bracket represents the thermal average. The quantity v_r is proportional to $[T(m_G + m_I)/m_G m_I]^{1/2}$ at a gas temperature T. In the case of the ion drifting in a gas mixture, the sum of Γ_{cn} for every neutral species gives the overall collision rate.

These general descriptions of drift velocity and mobility can apply in the case of ion transport in plasma so far as the collisions are considered to be elastic and result in no change in the internal state of ions. A modification of the equation of ionic center-of-mass motion, Eq. (2), is required in order to account for the collisions with charged particles which exhibit their drift motion along the external electric field. Although a rigorous treatment of this effect requires some detailed analysis of the microscopic collision process between charged particles, a modified equation of macroscopic motion of ions may be written in an approximated form by

$$m_I \frac{dv_{\text{c.m}}}{dt} = qE - \sum_k \Gamma_{c_k} m_I \{ v_{\text{c.m.}} - v_{d_k} \} \ , \tag{7}$$

where v_{d_k} is the drift velocity of the species labeled by k and Γ_{c_k} represents the rate of momentum loss due to collision with the species. It should be noted that, because the ion ensemble is considered, we include the effect of the resonant charge-exchange collision of an ion with its parent neutral atom into the rate of momentum loss, instead of treating it by separate decay and ionization processes.

2. State-specific drift velocity and mobility in plasma

In the case of the laser-Doppler measurement, the drift velocity of ions in a specific quantum state $|j\rangle$ is considered, and population and decay processes of the state must be taken into account in addition to purely kinetic phenomena described in the equation of ionic center-of-mass motion. Consider ions in the state $|j\rangle$ populated through $(j-1)$-step transitions via ionic states $|i\rangle$ $(i = 1, \ldots, j-1)$ after ionization, and let t_i be the duration that the ions spent in each state $|i\rangle$. The multistep transitions between ionic states considered here are transitions such as optical cascade transition and electronic stepwise transition. Assume that the drift velocity is measured instantaneously, at a moment t_j after the state $|j\rangle$ is populated by means of the laser-Doppler measurement of an absorption line due to transition between the state $|j\rangle$ and an ionic state $|e\rangle$. The transition cascade makes the acceleration time finite, and the resultant drift velocity does not exhibit its steady-state value. If the same rate of momentum loss, Γ_c, is assumed for all of the ionic states involved, the acceleration time t_a in Eq. (3) is given simply by the total duration of the transition cascade as

$$t_a = \sum_{i=1}^{j} t_i \ , \tag{8}$$

since the acceleration by the electric field is independent of the state of the ion. For the state-specific ensemble of ions, the distributions of t_i and t_j are given by the probability density

$$p_i(t_i) = \gamma_i e^{-\gamma_i t_i} \ , \quad i = 1, \ldots, j \ , \tag{9}$$

where γ_i is the relaxation rate of the state $|i\rangle$, including collisional transfer and other decay mechanisms, and is equal to the reciprocal of the effective lifetime τ_i of the state. For further detailed discussion, let us write γ_i as

$$\gamma_i = A_i + \gamma_{c_i} + \gamma_{g_i} \ , \tag{10}$$

where A_i and γ_{c_i} are the rates of spontaneous and collisional decay of the state $|i\rangle$, respectively, and γ_{g_i} is the rate of decay due to geometrical shape of the plasma, such as diffusion and drift in the direction transverse to the applied electric field. The last term γ_{g_i} has an effect when the transport of ions in a long-lived state is considered in a confined plasma. Equation (9) stands even when a portion of ions branches off the transition cascade considered. The center-of-mass velocity of the ion in the state $|j\rangle$ averaged over distribution of the acceleration time gives the state-specific drift velocity $v_d(j)$ as

$$\begin{aligned} v_d(j) &= \int_0^\infty \cdots \int_0^\infty \frac{qE}{m_I \Gamma_c} \left[1 - \exp\left[-\Gamma_c \sum_{i=1}^{j} t_i \right] \right] \\ &\quad \times \prod_{i=1}^{j} (\gamma_i e^{-\gamma_i t_i} dt_i) \\ &= \frac{\Gamma_c}{\Gamma_{ce}(j)} v_d \ , \end{aligned}$$

$$\Gamma_{ce}(j) = \Gamma_c \left[1 - \prod_{i=1}^{j} \left[\frac{\gamma_i}{\gamma_i + \Gamma_c} \right] \right]^{-1} \ , \tag{11}$$

where v_d is the steady-state drift velocity given by Eq. (4). This result indicates that the effect of population and decay processes on the drift motion of the ion ensemble in the state $|j\rangle$ can be reduced into the equation of center-of-mass motion, Eq. (2), by replacing the usual collision rate Γ_c with the effective collision rate $\Gamma_{ce}(j)$. In this sense, the state-specific ensemble of ions exhibits a steady-state motion which is very different from the usual kinetic steady state. In Eq. (11), the second term of $\Gamma_{ce}(j)$ represents such corrections due to population and decay processes of the ionic state $|j\rangle$.

Since the state-specific drift velocity in Eq. (11) is proportional to the applied electric field E, one can define an apparent mobility of the state-specific ensemble of ions by the factor of proportionality

$$\mu(j) = \frac{v_d(j)}{E} = \frac{q}{m_I \Gamma_{ce}(j)} = \frac{\Gamma_c}{\Gamma_{ce}(j)} \mu \ , \tag{12}$$

although it does not describe a steady state in the usual sense. The differences between the steady-state and the state-specific or apparent values are given by

$$\frac{\mu - \mu(j)}{\mu} = \frac{v_d - v_d(j)}{v_d} = \prod_{i=1}^{j} \left[\frac{\gamma_i}{\gamma_i + \Gamma_c} \right] \ . \tag{13}$$

So far, we assumed the state-independent collision rate Γ_c. The expression of $v_d(j)$ can be generalized by using state-dependent collision rates Γ_{c_i} of the state $|i\rangle$ as

$$\begin{aligned} v_d(j) = \int_0^\infty \cdots \int_0^\infty \frac{qE}{m_I} \sum_{i=1}^{j} \left\{ \frac{1}{\Gamma_{c_i}} [1 - e^{-\Gamma_{c_i} t_i}] \right. \\ \left. \times \exp\left[- \sum_{k=i+1}^{j} \Gamma_{c_k} t_k \right] \right\} \\ \times \prod_{l=1}^{j} (\gamma_l e^{-\gamma_l t_l} dt_l) \ . \end{aligned} \tag{14}$$

The state-specific drift velocity and apparent mobility approximate the steady-state values in the case in which at least one of the γ_i's considered in Eq. (11) is much smaller than Γ_c, or equivalently one of the states $|i\rangle$ has lifetime longer than the collisional mean free time τ_c, and steady-state condition is nearly achieved. These conditions apply for cases where the state $|j\rangle$ is the ionic ground or metastable state or where $|j\rangle$ is populated by a stepwise excitation through the ionic ground or metastable state. The state-specific drift velocity and apparent mobility in these cases are given by the effective collision rate

$$\frac{1}{\Gamma_{ce}(j)} \simeq \frac{1}{\Gamma_c} \left[1 - \prod_{\gamma_i \ll \Gamma_c} \left[\frac{\gamma_i}{\Gamma_c} \right] \right] \approx \frac{1}{\Gamma_c} \ . \tag{15}$$

By contrast, the idea of the state-specific drift velocity and apparent mobility is quite different from the usual concept of drift velocity and mobility when all of the states $|i\rangle$ $(i = 1, \ldots, j)$ are short-lived states and γ_i's are as large as Γ_c. In this case the transport of ions in the state $|j\rangle$ is transient at all conditions and gives $v_d(j)$ and $\mu(j)$ smaller than the steady-state values.

In the case where all of the γ_i's are much larger than Γ_c, the effective collision rate is given approximately by

$$\frac{1}{\Gamma_{ce}(j)} \simeq \sum_{i=1}^{j} \frac{1}{\gamma_i} = \sum_{i=1}^{j} \tau_i \ , \tag{16}$$

and the state-specific drift velocity and apparent mobility are determined by the sum of lifetimes of ionic states involved in the transition cascade. These conditions apply to the case where the state $|j\rangle$ is a highly excited state populated by a transition cascade via upper ionic states of short lifetime.

In the special case where the state $|j\rangle$ is populated by a direct ionization from a parent neutral atom, by Penning collision, for example, the effective collision rate is given by

$$\Gamma_{ce}(j) = \Gamma_c + \gamma_j \ , \tag{17}$$

and the state-specific drift velocity and apparent mobility

are determined by the lifetime of the ionic state considered.

In an actual plasma, a specified ionic state $|j\rangle$ may be populated by one or several of the ways classified above according to the condition of the plasma, and the laser measurement of drift velocity serves as a useful technique to study excitation and decay mechanisms of the ionic state. Even in the case where the state $|j\rangle$ has several independent ways of excitation with different excitation times, they can be separated, in principle, by means of numerical deconvolution of the Doppler profile into each Gaussian component of different central frequency. Feasibility of such deconvolution depends on the signal quality of the laser-Doppler measurement and the detailed knowledge about the line-shape function including hyperfine sublevels, isotope shifts, and so on.

As well as the population and decay mechanisms discussed above, the geometrical shape of the plasma has an effect on the transport property of long-lived ions when the plasma is confined in a relatively small envelope such as a thin discharge tube. In this case, the transverse diffusion and drift of ions followed by deposition and recombination at the container wall contribute to the decay rate γ_i of the state-specific ensemble of ions as in Eq. (10). As an example, for a positive column of a glow discharge in a thin cylindrical tube of inner radius R, the rate γ_g is determined by the ambipolar diffusion in the radial direction and succeeding deposition or recombination of ions at the tube wall. Provided that the center-of-mass velocity of ions is lost completely at the collisions with the tube wall, a simple calculation gives

$$\gamma_g = \frac{D_a}{p_G}\left[\frac{2.405}{R}\right]^2 , \tag{18}$$

where D_a is the ambipolar diffusion coefficient reduced to 1 torr at the experimental temperature and p_G is the gas pressure.

III. EXPERIMENTAL SETUP

A. Frequency-controlled diode laser

$Al_xGa_{1-x}As$ lasers used in this experiment were Mitsubishi ML3401 lasers operating on a single longitudinal mode with a spectral width of several tens of MHz (full width at half maximum). A precise control of the laser frequency was achieved by means of stabilization of diode temperature and injection current [8,9]. Typical values of temperature and current stability obtained were better than 10^{-3} K and 1 μA, respectively, which result in frequency fluctuation less than 1 MHz with a small frequency drift of several megahertz per minute in ordinary room-temperature operation. A ramp voltage, applied to the temperature stabilization electronics, sweeps the laser frequency over 10 GHz preserving the short-term stability. Typical rate of the frequency sweep is $\sim$35 MHz/s in this experiment. The temperature change of the laser diode is a useful measure of the swept frequency, being proportional to the frequency difference with a ratio of about 20 GHz/K; values were measured for each diode sample by using a Fabry-Pérot resonator of 2-GHz free spectral range. A change in the diode temperature is measured by a small thermistor as its resistance change which is converted to an output voltage by using a bridge circuit. A frequency shift of ionic resonance lines down to about 10 MHz can be resolved adopting the frequency control scheme of the diode laser. The resolution is much better than the Doppler width of a single resonance line and provides the feasibility of deconvolution of the Doppler profile into each Gaussian component in high accuracy. The linearity of the frequency scanning was confirmed by observing the hyperfine spectra of the Cs-D_2 line at 852.1 nm using $Al_xGa_{1-x}As$ lasers of the same type.

B. Experimental arrangement

The experimental arrangement is shown in Fig. 2. The beam from a tunable single-mode $Al_xGa_{1-x}As$ laser diode was circularly polarized and divided into two beams by a polarizing beam splitter. After each beam was propagated in opposite directions through a positive column, the absorption of the laser was measured by separate detecting systems. In order to improve the signal-to-noise ratio the laser beam was chopped and a lock-in detection was employed.

For the measurement of the drift velocity of Ca^+ ions, a discharge tube made of quartz was set in a furnace and heated to a specified temperature. An additional close-fitting cylindrical tube made of alumina with a length of 14 cm was inserted in the discharge tube. The length of the alumina tube almost fit the uniformly heated area of the furnace. Alumina tubes with various inner diameters $2R$ were used to change the diameter of the positive column. Grains of Ca with a size of less than 1 mm were placed in the alumina tube uniformly over the full length. As the Ca tended to react with the wall material, uniform placement of the grains was necessary to achieve a uniform vapor density of Ca over the length of the alumina

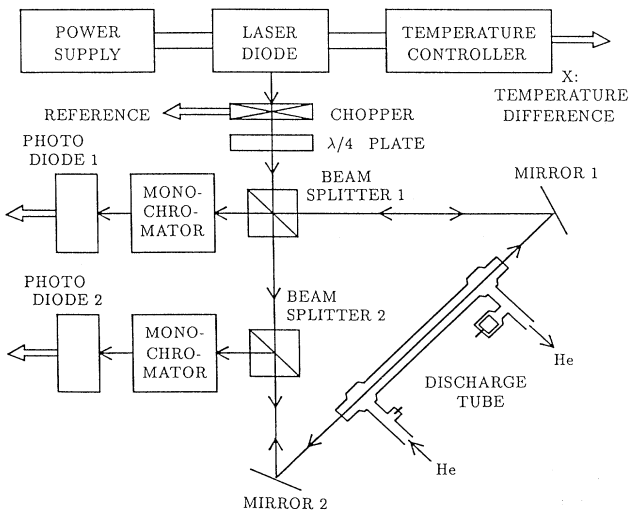

FIG. 2. Experimental arrangement.

tube. A constant Ca vapor pressure of 0.44 torr [10] was obtained during about 7 h at a gas temperature of 750 °C. After operation of the discharge for 5 h, the tube was cleaned and new grains of Ca were inserted. When the Ca vapor pressure was less than 0.1 torr at a gas temperature of less than 650 °C, the population density of the $3\,^2D_{3/2}$ state of Ca^+ ions was too low to measure the absorption with a good signal-to-noise ratio. For this reason, the experiments for Ca were made at gas temperatures around 750 °C.

The drift velocity of Cd^+ ions was measured with a discharge tube whose structure was almost the same as those generally used for He-Cd lasers [11] and inner diameter was 3.5 mm. A Cd reservoir or condenser was placed at the end of the positive column. The Cd evaporated from the reservoir was distributed uniformly over the positive column due to cataphoresis [12]. The experiments were made at temperatures around 250 °C and a helium pressure of 4.5 torr and the Cd vapor pressures p_{GCd} were around 10^{-3} torr [10], which are the actual conditions used for He-Cd lasers. One insertion of Cd grains kept the vapor pressure stable during a few experiments.

In both the Ca and Cd experiments, a buffer gas of helium was kept flowing slowly along the tube axis. It was confirmed that the flow speed was small enough not to disturb the ion drift. The experiments were made at helium gas pressures less than 25 torr. The ionic states used for observations of the drift velocity were $3\,^2D_{3/2}$ for Ca^+ and $6\,^2P_{3/2}$ for Cd^+, whose resonance wavelengths were 849.8 and 838.9 nm, respectively. One of the reasons why these ionic states were selected in the experiment is that the resonance wavelengths just fit the $Al_xGa_{1-x}As$ diode laser. Another important reason is that the $3\,^2D_{3/2}$ state is the metastable state of Ca^+ whereas, in contrast, the $6\,^2P_{3/2}$ is the highly excited state of Cd^+. Because the electric field strength is sensitively dependent on the atomic density of the vapor [13], the axial electric field in the positive column was simultaneously measured using electric probes inserted in the plasma. In the experiment with wider diameter tubes, the gas temperature in the plasma was also measured by insertion of a thermocouple covered with a glass sleeve.

IV. RESULTS AND DISCUSSIONS

As described above, the absorption spectra were measured with laser beams propagating in opposite directions. The drift velocity was calculated from the frequency difference between zero crossing points of the third-order differential curves of the spectra with respect to frequency, processed by a computer, and the state-specific mobility was estimated from the measured electric field.

A. Ca^+

The experimental result of the absorption spectra is shown in Fig. 3. The shape, which is very close to a single Gaussian profile, results from the facts that natural Ca has a nearly single isotope and Ca^+ ions in the $3\,^2D_{3/2}$ state drift with one velocity component. The drift velocity is simply obtained from the frequency difference between two absorption spectra by using Eq. (1).

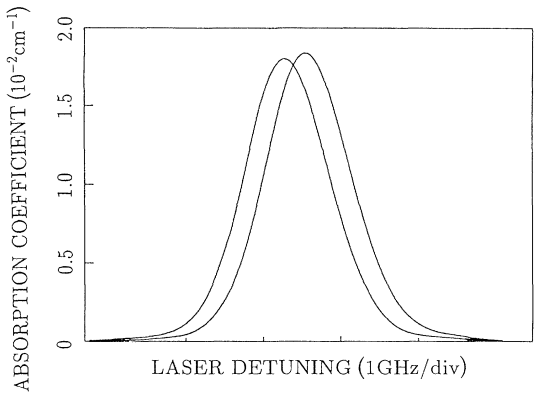

FIG. 3. The experimental result of the absorption spectra of Ca^+ ions in the $3\,^2D_{3/2}$ state measured by laser beams propagating in opposite directions. The experiment was made under the condition of tube inner diameter $2R$ of 11 mm, helium gas pressure p_G of 18 torr, discharge current I of 160 mA, and Ca^+ temperature T_i of 750 °C.

The results, as a function of radial position, are shown in Fig. 4. The radial profile of the absorption coefficient agreed well with the zeroth-order Bessel function which is shown by the solid curve in Fig. 4. The peak absorption coefficient is 0.009 cm^{-1} and the density of the $3\,^2D_{3/2}$ state at the center of the bore is estimated to be 3.9×10^{10} cm^{-3} with the value of the probability of the spontaneous emission [14]. The absorption coefficient is

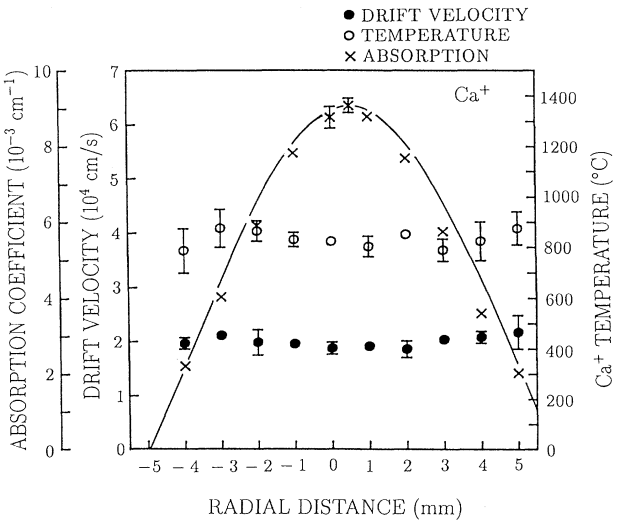

FIG. 4. Drift velocity, absorption coefficient, and temperature of Ca^+ ions in the $3\,^2D_{3/2}$ state as a function of radial distance measured from the roughly estimated tube center. The solid curve indicates the zeroth-order Bessel function. The experiment was made under the condition of $2R$ of 11 mm, I of 120 mA, and p_G of 9 torr.

high enough to measure the absorption profile in good signal-to-noise ratio. The drift velocity and the ion temperature remained almost constant with change in radial position. Similar results were obtained at the low gas pressure of 1 torr. These results verified that the plasma in this condition was described by Schottky's theory and that ambipolar diffusion determined the radial movement of the particles. The same measurement was made with a quartz tube instead of the alumina tube. Though the quartz is more reactive than alumina with Ca, the numerical values obtained here are quite the same as those shown in Fig. 4. The collision with the quartz wall simultaneously causes a loss of a Ca^+ ion due to a chemical reaction and a loss of its momentum. As the Ca grains are placed over the length of the inner tube, the loss of Ca is balanced with an evaporation from the grains and the Ca^+ density is kept constant in the plasma. The rate of the momentum loss by the collision with the wall is independent of the wall material and the change in material of the tube does not affect the movement of the ion averaged over the plasma length. If the experiment is made with the discharge tube used for Cd where the ion distributes due to cataphoresis, the result may be changed.

The experimental results also showed that the absorption coefficient, which is proportional to the population density of an ionic state, was linearly dependent on the discharge current and the helium pressure. This indicated that the Ca^+ ion in the $3\,^2D_{3/2}$ state was mainly excited from neutral Ca atoms by a single-step electron collision under these experimental conditions. The gas temperature measured by the thermocouple agreed with the ion temperature estimated from the Doppler width at all of the experimental conditions.

The mobilities of the Ca^+ ion in the $3\,^2D_{3/2}$ state estimated from Eq. (12) are plotted in Fig. 5 as a function of helium pressure. The ion temperature at a pressure of 18 torr for every tube of different inner diameter was kept constant at 750 °C by control of the input power to the furnace. Measurements were also made as a function of the input power to the furnace. The mobility decreased slightly with temperature. It shows, as discussed in a following section, that at the temperatures measured the Ca^+ ion transport is affected by the collision with Ca neutral atoms in addition to the collision with He atoms.

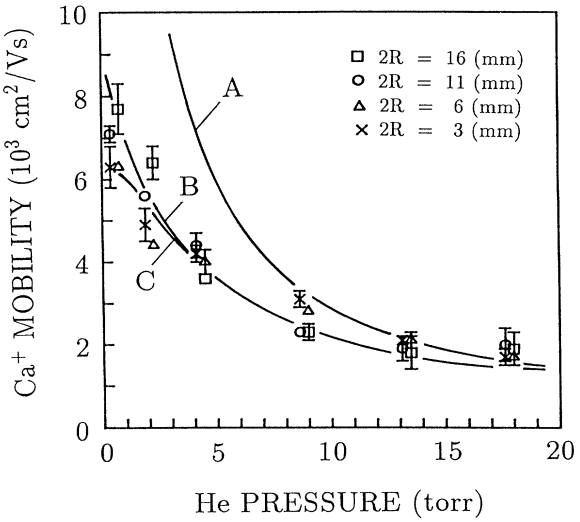

FIG. 5. Mobility of Ca^+ ions in the $3\,^2D_{3/2}$ state as a function of helium gas pressure at various values of $2R$. In the experiment I was 160 mA and T_i at 18 torr was kept constant at 750 °C. The vapor pressure of Ca was estimated to be 0.44 torr. The data obtained at diameters of 16 and 6 mm are plotted at a pressure of 0.5 torr higher than that used in the experiment in order to indicate clearly on the graph the values of mobility at different diameters. The lines A, B, and C show fitted curves (see text).

B. Cd^+

The experimental results for Cd^+ are shown in Figs. 6 and 7. A gas temperature of the positive column was kept constant and the Cd vapor pressure was of the order of 10^{-3} torr at the reservoir temperature used in this experiment.

For the case of Cd^+, the effective width of the measured absorption line profile was nearly 1.2 GHz which was much larger than the Doppler width calculated for a single line of Cd^+. One of the reasons is that a spectrum of Cd^+ is a superposition of frequency-shifted lines due to several isotopes. Another reason is that ions in the $6\,^2P_{3/2}$ state can be excited by several processes and as a result have different drift-velocity components due to different mobilities as described in a following section. Since the frequency shift estimated from the drift velocity is smaller than the width of the absorption profile, it is difficult to separately observe peaks based on different drift velocities in the absorption profile, and, however, the effective width of the absorption profile becomes larger than the width of a single line. Under these conditions each component of drift velocity can be separately estimated by means of the deconvolution of the absorp-

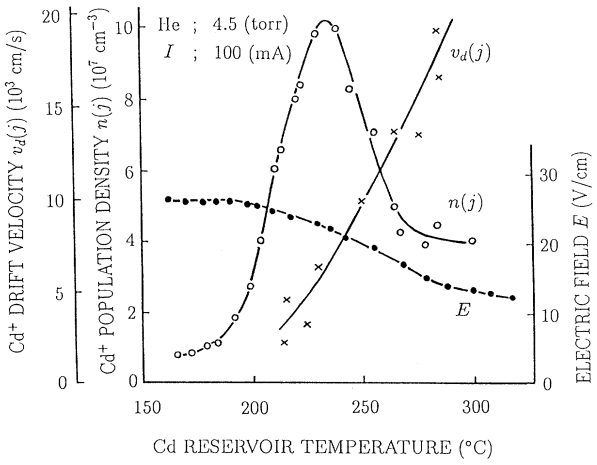

FIG. 6. Drift velocity $v_d(j)$ and population density $n(j)$ of Cd^+ ions in the $6\,^2P_{3/2}$ state and axial electric field E as functions of Cd reservoir temperature obtained with the tube of diameter 3.5 mm.

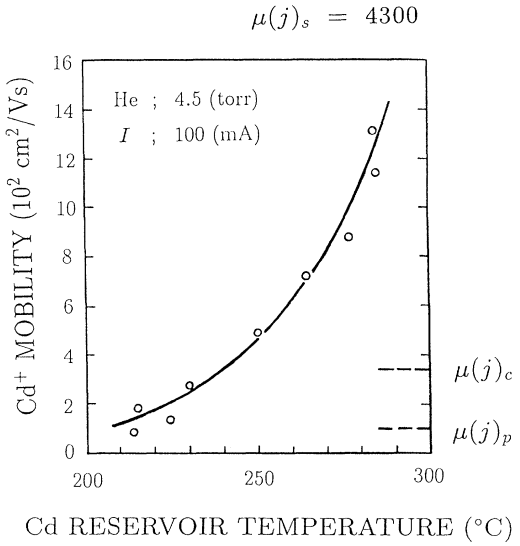

FIG. 7. Mobility $\mu(j)$ of Cd^+ ions in the $6\,^2P_{3/2}$ state as a function of Cd reservoir temperature. The quantities $\mu(j)_p$, $\mu(j)_c$, and $\mu(j)_s$ indicate mobilities calculated for different dominant processes in the excitation mechanism for the $6\,^2P_{3/2}$ state (see text). The values $\mu(j)_p$ and $\mu(j)_c$ are shown by broken lines; $\mu(j)_s$ is much larger than other results and is printed outside the graph.

tion line profile which is the superposition of line shapes. But in this paper the deconvolution was not performed because of the poor signal-to-noise ratio of the absorption signal and lack of detailed knowledge about the line-shape function based on the isotope shift of Cd^+. The former is due to the low ion density in the highly excited state. The drift velocity of Cd^+ shown in Fig. 6 was estimated, therefore, from the shift of the frequency at a peak of the measured absorption profile and the value indicates the average of drift velocities due to the different excitation processes under the consideration that each isotope has the same drift velocity.

The drift velocity and the mobility were dramatically increased with the temperature of the reservoir. The population density of the $6\,^2P_{3/2}$ state of Cd^+ shown in Fig. 6 [curve $n(j)$] has a maximum at a temperature of about 230 °C. The electric field measured (curve E) shows a significant decrease with increase in temperature from 200 to 300 °C. Results similar to ours for both the population density of the upper state of Cd^+ in the laser transition and the electric field have been reported in previous works analyzing the excitation mechanism of the He-Cd laser [15–17]. The temperature dependences of the drift velocity and the mobility are considerably different from the results measured for Ca. The discussions in Refs. [15–17] suggest that the higher-energy states of Cd^+ are excited by a complicated scheme that mixes many processes; the excitation mechanism and therefore the effective collision rate $\Gamma_{ce}(j)$ are considerably affected by the discharge conditions, and the apparent mobility of the Cd^+ ions in the $6\,^2P_{3/2}$ state varies with the changes in the discharge conditions as discussed in the following.

C. Analysis of mobility

1. Ca^+ in metastable state

The $3\,^2D_{3/2}$ state of Ca^+ is the metastable state and is mainly excited by an electronic collision. Therefore the momentum-loss collision rate Γ_c is usually larger than the decay rate γ_j and the apparent state-specific mobility of ions in the $3\,^2D_{3/2}$ state is given by Eqs. (12) and (15) or equivalently given by Eq. (5). The experimental results of the mobility shown in Fig. 5 are again plotted in Fig. 8 on a logarithmic scale. The results in Fig. 8 approximately converge to a straight line with a slope of -1 at pressures above 10 torr. It seems that the momentum-loss collision only with helium is dominant at these pressures and its collision rate Γ_{cn} given by Eq. (6) is denoted by $\Gamma_{cn\mathrm{He}}$. The cross section for this momentum-loss collision, $\langle\sigma_{cn\mathrm{He}}\rangle$, is estimated to be 3×10^{-15} cm^2 from the slope of the straight line. The geometrical cross section $\pi(r_{\mathrm{He}}+r_{\mathrm{Ca}})^2$, where r_{He} and r_{Ca} are the atomic radii of helium and calcium, respectively, calculated from the published data for the radii [18] is 3.4×10^{-15} cm^2, which is in good agreement with the value obtained here. Curve A in Fig. 5 is the same as the straight line in Fig. 8 and indicates the mobility calculated with a cross section $\langle\sigma_{cn\mathrm{He}}\rangle$ of 3×10^{-15} cm^2 for the case of collisions only with helium.

At pressure lower than 10 torr in Fig. 8, the mobility does not fit the line with a slope of -1. At these pressures the effect on the mobility of collision with Ca atoms must be considered, because the Ca vapor pressure cannot be ignored in comparison with the He pressure. In this case the momentum-loss collisions with both He and Ca atoms are included in Eq. (6) and Γ_{cn} is given by

$$\Gamma_{cn}=\Gamma_{cn\mathrm{He}}+\Gamma_{cn\mathrm{Ca}}\ , \tag{19}$$

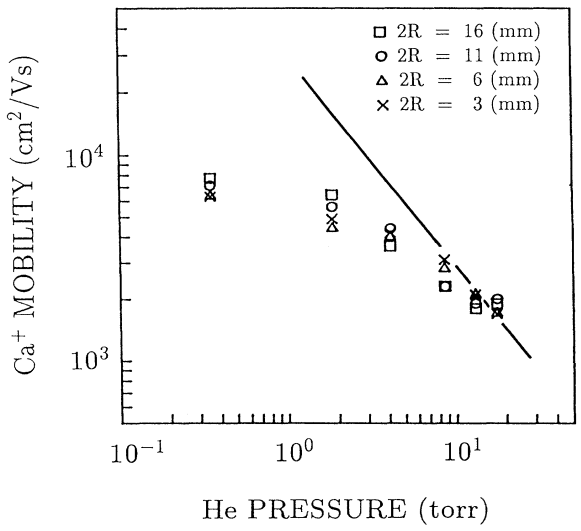

FIG. 8. Mobility of Ca^+ ions in the $3\,^2D_{3/2}$ state shown in Fig. 5 is plotted on a logarithmic scale. The experimental data obtained at higher pressures fit a straight line with a slope of -1.

where $\Gamma_{cn\mathrm{Ca}}$ is the rate that the Ca^+ ion in the $3\,^2D_{3/2}$ state loses its momentum by collisions with neutral Ca atoms such as elastic collision and resonant charge-exchange collision. The mobilities are calculated with various values of the cross section $\langle \sigma_{cn\mathrm{Ca}} \rangle$ for collision with calcium at the cross section $\langle \sigma_{cn\mathrm{He}} \rangle$ of fixed value 3×10^{-15} cm^2. Curve *B* in Fig. 5 is the best fit to the experimental results obtained with tubes of inner diameter 11 and 16 mm. From the best fit the cross section $\langle \sigma_{cn\mathrm{Ca}} \rangle$ is estimated to be 9.0×10^{-15} cm^2 which is larger than the geometrical cross section $\pi(r_{\mathrm{Ca}}+r_{\mathrm{Ca}})^2$ of 5.5×10^{-15} cm^2 [18]. This difference may be explained with the consideration that the value of $\langle \sigma_{cn\mathrm{Ca}} \rangle$ obtained here is affected by both cross sections for elastic collisions and resonant charge-exchange collisions.

If it is assumed that the cross sections $\langle \sigma_{cn\mathrm{He}} \rangle$ and $\langle \sigma_{cn\mathrm{Ca}} \rangle$ obtained here for the $3\,^2D_{3/2}$ metastable state of Ca^+ ions are equal to the cross sections for the ionic ground state, mobilities of Ca^+ ions in the ground state in pure helium gas, $\mu_{0\mathrm{He}}$, and in pure calcium gas, $\mu_{0\mathrm{Ca}}$, under the condition of 760 torr and 300 K, are estimated to be 20 and 2.7 cm^2/V s, respectively. These values cannot be compared with experimental results, because data for Ca^+ ions have not been published previously. However, values of $\mu_{0\mathrm{He}}$ and $\mu_{0\mathrm{Ca}}$ can be estimated to be 22 and 2.0 cm^2/V s, respectively, from a series of the published data for the mobility of other ions with different mass numbers [2,19,20] and agree well with the state-specific mobilities estimated here.

At pressures lower than 3 torr, the experimental error is rather large because of poor signal-to-noise ratio due to the small absorption coefficient. However, the result shows that the apparent mobility decreases with decrease in the tube diameter. This is caused by the momentum loss of the ion on collision with the wall after it has diffused to the wall in the radial direction. Under this condition $\gamma_j \approx \gamma_{gj}$ is comparable to Γ_{cn} and the apparent mobility should be calculated from Eqs. (10) and (17) by including the term γ_{gj} due to diffusion, in addition to $\Gamma_{cn\mathrm{He}}$ and $\Gamma_{cn\mathrm{Ca}}$. Curve *C* in Fig. 5 shows the calculated fit to the experimental results obtained for the tube of diameter 3 mm, from which the best-fit estimate for the diffusion coefficient D_a of Ca^+ is 3.0×10^3 cm^2 s^{-1} torr. In the calculation, for simplicity, the total gas pressure is used as p_G in Eq. (18). If it is assumed that D_a is proportional to $T^{1/2}$, D_{a0} at 1 torr and 300 K is 1.6×10^3 cm^2/s. The mobility calculated for tubes for larger diameter, 11 and 16 mm, taking the γ_{gj} term into account in addition to Γ_{cn} is the same as the result shown by curve *B* in Fig. 5. As γ_{gj} is proportional to R^{-2}, the effect of γ_{gj} on the mobility for the tubes of wider bore can be ignored in comparison with the effect of Γ_{cn}.

In our experiments with Ca, the mobility is found to be independent of the discharge current. Throughout the present experiment the discharge current was less than 200 mA and the density of the charged particles was estimated to be around 10^{12} cm^{-3}. This density is too low for the charged particles to have a measurable effect on the mobility through momentum-loss collisions under these experimental conditions.

2. Cd^+ in highly excited state

The mobility of Cd^+ ions in the $6\,^2P_{3/2}$ excited state should be considered from Eq. (12) and the excitation and the decay processes become important in addition to the momentum-loss collision. Under this condition Cd vapor pressure is very low and the rate of collisions with parent Cd atoms, such as elastic and resonant charge-exchange collisions, is neglected in comparison with the rate of elastic collisions with He atoms. It has been confirmed that Cd^+ ions in the upper and lower states of the laser transition are excited mainly by stepwise electron collisions and Penning collisions rather than by direct electron collision [15–17]. The excitation mechanisms of Cd^+ in other excited states have not been discussed in detail previously. An analysis of the excitation probability for the $6\,^2P_{3/2}$ state is more complicated than that for the states of the laser transition, because the $6\,^2P_{3/2}$ state can also be excited by the radiative cascade from higher excited states of Cd^+ which are ionized by a charge-transfer collision with helium ions (hereafter we call this process a charge transfer followed by cascade), besides being excited by stepwise electron collision, Penning collision, and direct electron collision. It is necessary to estimate quantitatively the probability of each process in order to discuss the apparent state-specific mobility of Cd^+ ions in the $6\,^2P_{3/2}$ state measured here as shown in Fig. 7.

One of the excitation mechanisms to the $6\,^2P_{3/2}$ state of Cd^+ may be Penning collisions with He atoms in higher excited states and Cd atoms. The rate of Penning collisions *P* is given by $\langle \sigma_p v_r \rangle n^*_{\mathrm{He}} n_{G\mathrm{Cd}}$, where σ_p is the cross section, n^*_{He} is the sum of the population densities of the He excited states whose energies are higher than that of the $6\,^2P_{3/2}$ state of Cd^+ and $n_{G\mathrm{Cd}}$ is the Cd vapor density.

The charge transfer followed by cascade is probably as effective as the Penning excitation. In the case of the charge transfer followed by cascade the $6\,^2P_{3/2}$ state is populated by a one- or two-cascade transition after the $6\,^2F$, $8\,^2D$, and $9\,^2S$ states of Cd^+ ions are ionized by the charge-transfer collision with a helium ground-state ion [21]. The excitation rate of the charge transfer followed by cascade *C* to the $6\,^2P_{3/2}$ is given by $\langle \sigma_c v_r \rangle n^+_{\mathrm{He}} n_{G\mathrm{Cd}} q$, where σ_c is the cross section, n^+_{He} is the population density of helium ions in the ground state, and *q* is the branching ratio of the cascade transition from the $6\,^2F$, $8\,^2D$, or $9\,^2S$ state to the $6\,^2P_{3/2}$ state. Other excitation mechanisms are thought to be direct and stepwise excitations by electron collision whose rates *D* and *S* are given by $\langle \sigma_{ed} v_e \rangle n_e n_{G\mathrm{Cd}}$ and $\langle \sigma_{es} v_e \rangle n_e n^+_{\mathrm{Cd}}$, respectively, where σ_{ed} and σ_{es} are the cross sections for the collision, v_e is the electron velocity, and n^+_{Cd} is the population density of Cd^+ ions in the ground state.

It is worthwhile to estimate these excitation rates' dependence on Cd vapor density in order to analyze the change in mobility shown in Fig. 7. Table I reports the calculated *P*, *C*, *S*, and *D* values in addition to the plasma parameters at different temperatures. The plasma parameters and the particle densities listed in Table I are inferred from the data measured by using the same type of discharge tube as ours [13,22,23]. The result that the

TABLE I. Plasma parameters; average electron energy V_e (eV), and densities n_{GCd}, n_e, n^+_{Cd}, n^+_{He}, and n^*_{He} (10^{12} cm^{-3}) and excitation rates populating the $6\,^2P_{3/2}$ state of Cd^+; Penning collision P, charge transfer followed by cascade collision C, stepwise electron collision S, and direct electron collision D (10^{13} cm^{-3}s^{-1}) at different temperatures T (°C). R_{p0} and R_{c0} are the rates for Penning and charge transfer followed by cascade excitations, respectively, at $T=195$ °C.

T	n_{GCd}	V_e	n_e	n^+_{Cd}	n^+_{He}	n^*_{He}	P	C	S	D
195	5	5.7	0.9	0.2	0.70	2.5	R_{p0}	R_{c0}	7	0.19
205	10	5.6	0.9	0.4	0.50	1.8	$1.4R_{p0}$	$1.4R_{c0}$	14	0.34
237	50	4.7	1.2	1.1	0.05	0.3	$1.2R_{p0}$	$0.7R_{c0}$	30	0.72
250	100	4.4	1.3	1.3	0.01	0.1	$0.8R_{p0}$	$0.3R_{c0}$	30	0.95

values of n^+_{He} and n^*_{He} decrease with increase in temperature is caused by the fact that the electric field E and the average electron energy V_e must decrease with increase in Cd vapor density in order to keep a discharge current constant, because inelastic collisions of electrons with Cd atoms of low ionization energy occur more frequently as the Cd atom density increases.

The rate coefficients $\langle \sigma_p v_r \rangle$ and $\langle \sigma_c v_r \rangle$ are almost independent of the reservoir temperature, but there are no numerical data on the cross sections σ_p and σ_c to the state. Therefore the excitation rates P and C are shown in Table I only as a dependence on temperature. It is difficult to determine which excitation rate P or C is larger. The values of P and C decrease further with increase in vapor density at temperatures higher than 250 °C.

The rate coefficient of the direct and stepwise electronic collisions $\langle \sigma_{ed} v_e \rangle$ and $\langle \sigma_{es} v_e \rangle$ are strongly dependent on average electron energy and therefore on temperature. These rates listed in Table I are calculated with the consideration that the threshold energy V_{id} for the direct excitation from the neutral ground state to the $6\,^2P_{3/2}$ state is 21 eV, the threshold energy V_{is} for the stepwise excitation from the ionic ground state is 12 eV, and the electron velocity distribution is Maxwellian. The cross section for the stepwise excitation σ_{es} to the $6\,^2P_{3/2}$ state is roughly estimated to be 3×10^{-17} cm^2 from the facts that the electronic collision cross section for an optical allowed transition is proportional to an oscillator strength [18] and the value of σ_{es} to the $5\,^2P_{3/2}$ state is equal to 2.5×10^{-15} cm^2 [24].

The cross section for the direct excitation σ_{ed} to the $6\,^2P_{3/2}$ state is 4×10^{-19} cm^2 which is larger than that to the other highly excited state of Cd^+ [25,26]. However, the threshold energy V_{id} for the $6\,^2P_{3/2}$ state is much larger than the average electron energy and the rate coefficient for the direct electron collision $\langle \sigma_{ed} v_e \rangle$ is smaller by three orders of magnitude than $\langle \sigma_{es} v_e \rangle$ for stepwise collision. It is thus reasonable to ignore the excitation by direct electron collision in comparison with the excitation by stepwise electron collision, even if n_{GCd} is larger by one or two orders of magnitude than n^+_{Cd}. Therefore the direct electron collision cannot be a dominant excitation process. The numerical calculation as shown in Table I indicates that the Penning and the charge-transfer followed by cascade excitation rates for the $6\,^2P_{3/2}$ state, P, and C, become maximum at temperatures around 215 °C which are lower by about 40 °C than a temperature at which the stepwise excitation rate S becomes maximum. It is apparent that the excitation rates are considerably dependent on plasma parameters under the experimental condition of the Cd vapor density and the percentage of the excitation due to the stepwise electron collision increases with the temperature. A similar change in excitation mechanism has been shown for the upper level of a He-Cd laser transition [16].

If the excitation for the $6\,^2P_{3/2}$ state of Cd^+ ions is ensured to be 100% by Penning collision process, ions in the $6\,^2P_{3/2}$ state are directly excited from the neutral ground state of Cd atoms and the effective collision rate Γ_{ce} is given by Eq. (17). The probability A_j of the radiative decay of the $6\,^2P_{3/2}$ is 8×10^7 s^{-1} [27]. At the pressure and tube radius used in this experiment, the collisional decay rate γ_{cj} and the decay rate by diffusion γ_{gj} can be neglected in Eq. (10) in comparison with A_j. The quantity of $\Gamma_{cn\mathrm{He}}$ is calculated to be about 0.2×10^7 s^{-1} at 4.5 torr and 500 K, when $\langle \sigma_{cn\mathrm{He}} \rangle$ is assumed to be 3×10^{-15} cm^2, as calculated from the atomic radii [18]. Therefore $\Gamma_{ce}(j)$ is equal to 8.2×10^7 s^{-1} which is mainly determined by the radiative decay rate and the quantity of the apparent mobility is different from the mobility in the usual sense obtained at the steady state. For the case of 100% Penning excitation, the apparent mobility at 4.5 torr and 500 K, denoted by $\mu(j)_p$, is estimated to be 100 cm^2/V s by using Eq. (12).

Next if it is assumed that Cd^+ ions in the $6\,^2P_{3/2}$ state are excited at 100%, for example, from the $6\,^2F$ state by charge transfer followed by cascade, $1/\Gamma_{ce}(j)$ is approximately given by Eq. (16) to be 40 ns which is the sum of the radiative lifetimes of the $6\,^2F_{7/2}$ (24 ns), of the $6\,^2D_{5/2}$ (4 ns), and of the $6\,^2P_{3/2}$ state (12 ns) [27]. Then, the apparent mobiliby for 100% charge transfer followed by cascade, denoted by $\mu(j)_c$, is estimated to be 340 cm^2/V s. When the $6\,^2P_{3/2}$ state is populated by charge transfer followed by cascade through the $8\,^2D_{5/2}$ or $9\,^2S_{1/2}$ state, the apparent mobility is calculated to be 210 or 290 cm^2/V s, respectively. These values are slightly dependent on the initial Cd^+ state populated by the charge-transfer collision with helium ions. In the above estimation of $\mu(j)_p$ and $\mu(j)_c$, the calculated radiative transition probabilities [27] are used, because there are no experimental data of transition probabilities for the higher excited states of Cd^+.

When the ion in the $6\,^2P_{3/2}$ state is assumed to be ex-

cited from the ground state of Cd^+ by the process of stepwise electron collision, $\Gamma_{ce}(j)$ is equal to the collision rate of the ion in the ground state, $\Gamma_{cn\mathrm{He}}=0.2\times10^7\ \mathrm{s}^{-1}$, as shown by Eq. (15). Under this condition, the mobility $\mu(j)_s$, which is equivalent to the usual definition of mobility for the ground-state Cd^+ ion in helium, is calculated to be 4300 $\mathrm{cm}^2/\mathrm{V\,s}$. The value of $\mu(j)_s$ corresponds to a mobility of 20 $\mathrm{cm}^2/\mathrm{V\,s}$ at 760 torr and 300 K. Even if ions drift with different velocity components due to different mobilities such as $\mu(j)_p$ and $\mu(j)_s$, it is difficult, as described in the preceding section, to separately observe each component of drift velocity in the absorption profile.

The estimated values of $\mu(j)_p$ and $\mu(j)_c$ are plotted as the broken lines in Fig. 7. The value of $\mu(j)_s$ is outside the range of the graph, but the experimental results obviously show that at high temperatures the mobility approaches the value of $\mu(j)_s$. The temperature dependence of the average value of the apparent state-specific mobilities measured from the experiments is interpreted by the hypothesis that, for the $6\,^2P_{3/2}$ state in Cd^+, excitations by Penning collision and charge transfer followed by cascade are dominant at lower temperatures whereas the excitation by stepwise electron collisions becomes the main process at higher temperatures. The change of the population density in the $6\,^2P_{3/2}$ state as shown in Fig. 6 suggests the change in excitation or destruction mechanism as temperature increases and this hypothesis can roughly explain the approximate change of the density. It is realized from the numerical calculation of the excitation rates as shown in Table I that this hypothesis may be correct when both rate coefficients of the Penning collision $\langle \sigma_p v_r \rangle$ and the charge transfer followed by cascade $\langle \sigma_c v_r \rangle q$ are of the order of 10^{-11} cm^3/s. These values are very reasonable in comparison with the experimental results obtained for other states [21,28,29]. In this case the excitation rates of Penning collision and charge transfer followed by cascade at temperature of 195 °C in Table I, R_{p0} and R_{c0}, are estimated to be several tens of 10^{13} $\mathrm{cm}^{-3}\,\mathrm{s}^{-1}$. The temperature dependence of the average value of apparent mobility shown in Fig. 7 is roughly explained by the change in excitation mechanisms due to the change in the vapor density.

V. CONCLUSION

The state-specific drift velocity and the apparent mobility of Cd^+ and Ca^+ ions in an excited state in the positive column of a helium dc discharge have been precisely measured under various conditions. The drift velocity was directly obtained from the shift of the resonance frequency due to the Doppler effect by using a tunable and stable diode laser. For the case of Ca^+ ions in the $3\,^2D_{3/2}$ metastable state, the apparent state-specific mobility decreases not only with the helium density but also with the calcium density, since the vapor pressure is close to the helium pressure at the temperature used. From the result the cross sections of the momentum-loss collisions with helium and calcium have been estimated. These values are almost the same as the cross sections calculated from the atomic radii. The mobilities at 760 torr and 300 K calculated from the value of the cross section estimated in the present experiment are in good agreement with values predicted from data for other ions in the ground state, which are usually obtained from drift-tube experiments. It has been confirmed that the mobility of ions in the metastable state measured by using a tube of larger diameter was not affected by excitation and decay processes. When a tube of narrow diameter was used in the experiment, however, the apparent mobility was affected by the radial diffusion of the ions. The ambipolar diffusion coefficient could then be roughly estimated from the value of mobility for a particular diameter of the tube.

It has been shown from the experimental results that the average of the apparent state-specific mobilities of Cd^+ ions in the $6\,^2P_{3/2}$ state increases considerably with the reservoir temperature. This dependence can be explained by the change in the excitation mechanism, i.e., at lower temperatures the ions in the $6\,^2P_{3/2}$ state are mainly excited by Penning collisions with helium atoms in highly excited states in addition to charge transfer followed by cascade, whereas at higher temperatures the stepwise electron collisions from the ionic ground state become the dominant process in the excitation mechanism. It is concluded from these results that the drift velocity and the mobility of an excited-state ion with a lifetime of less than 100 ns are significantly dependent on the excitation and the decay processes and their values are different from values corresponding to the usual definition for the ground-state ion.

The spectroscopic method using a diode laser also provides a means of obtaining precise measurements of the ion temperature in a plasma. In addition to studies of the effects of charged-particle collisions on mobility, it is also of interest to measure ion temperature distributions in various types of discharge plasmas. These measurements will give important information on the movement of particles in plasmas.

ACKNOWLEDGMENT

The authors would like to express their thanks to Masahito Yamaguchi for cordial technical assistance.

*Present address: Pioneer Co. Ltd., Saitama 350-02, Japan.
†Present address: Toshiba Lighting and Technology Co. Ltd., Yokosuka 237, Japan.
‡Present address: Asahi Chemical Industry Co. Ltd., Shizuoka 416, Japan.

[1] S. C. Brown, *Basic Data of Plasma Physics, 1966,* 2nd ed. (MIT, Cambridge, MA, 1967), Chap. 4.
[2] E. A. Mason and E. W. McDaniel, *Transport Properties of Ions in Gases* (Wiley, New York, 1988).
[3] L. D. Mash, B. M. Rabkin, and B. V. Rybakov, Pis'ma Zh. Eksp. Teor. Fiz. **13**, 240 (1971) [JETP Lett. **13**, 169 (1971)].
[4] K. Watanabe, S. Watanabe, and T. Sakurai, J. Appl. Phys. **52**, 3255 (1981).
[5] N. N. Haese, F. Pan, and T. Oka, Phys. Rev. Lett. **50**,

1575 (1983).
[6] A. C. G. Mitchell and M. W. Zemansky, *Resonance Radiation and Excited Atoms,* 3rd ed. (Cambridge University, Cambridge, England, 1971), Chap. 3.
[7] E. W. McDaniel, *Collision Phenomena in Ionized Gases* (Wiley, New York, 1964), Appendix 2, pp. 701–726.
[8] H. Hori, Y. Kitayama, M. Kitano, T. Yabuzaki, and T. Ogawa, IEEE J. Quantum Electron. **QE-19**, 169 (1983).
[9] H. Hori, K. Endo, E. Kono, and T. Sakurai, J. Appl. Phys. **60**, 2231 (1986).
[10] *American Institute of Physics Handbook,* 3rd ed., edited by D. E. Gray (McGraw-Hill, New York, 1972), Chap. 4.
[11] J. P. Goldsborough, Appl. Phys. Lett. **15**, 156 (1969).
[12] T. P. Sosnowski, J. Appl. Phys. **40**, 5138 (1969).
[13] J. K. Mizeraczyk, IEEE J. Quantum Electron. **QE-11**, 218 (1975).
[14] W. L. Wiese, M. W. Smith, and B. M. Miles, *Atomic Transition Probabilities,* Natl. Bur. Stand. (U.S.), No. NSRDS-NBS 22 (U.S. G.P.O., Washington, DC, 1969), Vol. II, p. 251.
[15] M. Mori, M. Murayama, T. Goto, and S. Hattori, IEEE J. Quantum Electron. **QE-14**, 427 (1978).
[16] T. Goto and T. Sakurai, J. Phys. D **15**, 2413 (1982).
[17] C. Boulmer-Leborgne, B. Dubreuil, and G. Gousset, J. Phys. D **20**, 579 (1987).
[18] C. W. Allen, *Astrophysical Quantities,* 3rd ed. (Athlone, London, 1973).
[19] M. A. Biondi and L. M. Chanin, Phys. Rev. **94**, 910 (1954).
[20] L. M. Chanin and M. A. Biondi, Phys. Rev. **107**, 1219 (1957).
[21] A. R. Turner-Smith, J. M. Green, and C. E. Webb, J. Phys. B **6**, 114 (1973).
[22] J. K. Mizeraczyk, J. Appl. Phys. **46**, 1847 (1975), and unpublished.
[23] M. Mori, K. Takasu, T. Goto, and S. Hattori, J. Appl. Phys. **48**, 2226 (1977).
[24] K. Hane, T. Goto, and S. Hattori, Phys. Rev. A **27**, 124 (1983).
[25] T. Goto, K. Hane, M. Okuda, and S. Hattori, Phys. Rev. A **27**, 1844 (1983).
[26] T. Goto, K. Hane, and S. Hattori, Phys. Rev. A **29**, 111 (1984).
[27] J. M. Green and C. E. Webb, J. Phys. B **8**, 1484 (1975); C. E. Webb (private communication).
[28] L. A. Riseberg and L. D. Schearer, IEEE J. Quantum Electron. **QE-7**, 40 (1971).
[29] S. Inaba, T. Goto, and S. Hattori, J. Phys. D **15**, 35 (1982).